

Northwest Pacific Anticyclonic Anomalies during Post–El Niño Summers Determined by the Pace of El Niño Decay

WENPING JIANG

State Key Laboratory of Numerical Modeling for Atmospheric Sciences and Geophysical Fluid Dynamics, Institute of Atmospheric Physics, Chinese Academy of Sciences, Beijing, and College of Oceanography, Hohai University, Nanjing, China

GANG HUANG

State Key Laboratory of Numerical Modeling for Atmospheric Sciences and Geophysical Fluid Dynamics, Institute of Atmospheric Physics, Chinese Academy of Sciences, Beijing, Laboratory for Regional Oceanography and Numerical Modeling, Qingdao National Laboratory for Marine Science and Technology, Qingdao, Joint Center for Global Change Studies, Beijing, and University of Chinese Academy of Sciences, Beijing, China

PING HUANG

State Key Laboratory of Numerical Modeling for Atmospheric Sciences and Geophysical Fluid Dynamics, Institute of Atmospheric Physics, Chinese Academy of Sciences, and Joint Center for Global Change Studies, and Center for Monsoon System Research, Institute of Atmospheric Physics, Chinese Academy of Sciences, Beijing, China

RENGUANG WU AND KAIMING HU

State Key Laboratory of Numerical Modeling for Atmospheric Sciences and Geophysical Fluid Dynamics, Institute of Atmospheric Physics, Chinese Academy of Sciences, and Center for Monsoon System Research, Institute of Atmospheric Physics, Chinese Academy of Sciences, Beijing, China

WEI CHEN

State Key Laboratory of Numerical Modeling for Atmospheric Sciences and Geophysical Fluid Dynamics, Institute of Atmospheric Physics, Chinese Academy of Sciences, Beijing, China

(Manuscript received 16 November 2018, in final form 2 March 2019)

ABSTRACT

This study investigates the characteristics and maintaining mechanisms of the anomalous northwest Pacific anticyclone (NWPAC) following different El Niño decaying paces. In fast decaying El Niño summers, the positive SST anomalies in the tropical central-eastern Pacific (TCEP) have transformed to negative, and positive SST anomalies appear around the Maritime Continent (MC), whereas in slow decaying El Niño summers, positive SST anomalies are present in the TCEP and in the tropical Indian Ocean (TIO). During fast decaying El Niño summers, the cold Rossby wave in response to the negative TCEP SST anomalies has a primary contribution to maintaining the NWPAC anomalies. The warm Kelvin wave response and enhanced Hadley circulation anomalies forced by the positive MC SST anomalies also facilitate developing the NWPAC anomalies. During slow decaying El Niño summers, the warm Kelvin wave anchored over the TIO plays a crucial role in sustaining the NWPAC anomalies, while the warm Rossby wave triggered by the positive TCEP SST anomalies weakens the western part of the NWPAC anomalies. The southwesterly anomalies of the NWPAC anomalies during fast decaying El Niño summers can reach to higher latitudes than those during slow decaying El Niño summers. Correspondingly, positive rainfall anomalies appear in northern China and the Yangtze River basin in fast decaying El Niño summers but are only distributed in the Yangtze River basin in slow decaying El Niño summers. This study implies that the El Niño decaying pace is a key factor in East Asian summer climate.

Corresponding authors: Dr. Ping Huang, huangping@mail.iap.ac.cn; Dr. Gang Huang, hg@mail.iap.ac.cn

DOI: 10.1175/JCLI-D-18-0793.1

© 2019 American Meteorological Society. For information regarding reuse of this content and general copyright information, consult the [AMS Copyright Policy \(www.ametsoc.org/PUBSReuseLicenses\)](https://www.ametsoc.org/PUBSReuseLicenses).

1. Introduction

El Niño–Southern Oscillation (ENSO) is the largest climate signal on interannual time scales and has pronounced impacts on global weather and climate (Horel and Wallace 1981, 1982; Ropelewski and Halpert 1987; Lau and Nath 1996; Webster et al. 1998). It is recognized as a primary predictor determining the interannual variability of the summer climate over the East Asia (Fu and Ye 1988; Huang and Wu 1989; Chang et al. 2000; Chou et al. 2009; Lin and Lu 2009; Zhang et al. 2016). Compared with the anomalies during ENSO developing summers, the northwest Pacific summer monsoon (NWPSM) anomalies occurring during ENSO decaying summers are much more pronounced (Xie et al. 2016). A low-level anomalous anticyclone over the northwest Pacific (NWP) develops in El Niño mature winter and persists to the following spring and summer, which plays a crucial role in linking ENSO and summer climate in East Asia and the NWP (Huang and Wu 1989; Zhang et al. 1996, 1999; Wu et al. 2003; Lau and Nath 2006).

Several mechanisms have been proposed to explain how ENSO, which typically peaks in boreal winter and decays afterward, can still exert an influence on the NWP circulation anomalies during the following summer. These mechanisms emphasize that sea surface temperature (SST) anomalies induced by ENSO in multiple oceans are important in producing the delayed influence. The local cold SST anomalies in the NWP force an anomalous NWP anticyclone (NWPAC) by triggering a cold atmospheric Rossby wave during the El Niño mature winter, then the northeasterly anomalies to the southeastern flank of the NWPAC in turn enhance wind and cool local SST (Wang et al. 2000; Wang et al. 2003), and finally the local positive air–sea feedback maintains the NWPAC to the following spring and early summer (Wu et al. 2010). A basinwide warming in the tropical Indian Ocean (TIO) induced by El Niño through atmospheric and oceanic processes (Klein et al. 1999; Chiang and Sobel 2002; Xie et al. 2002; Chiang and Lintner 2005; Du et al. 2009) can also prolong the El Niño impacts on NWPAC through a Matsuno–Gill pattern in the tropospheric temperature. A warm atmospheric Kelvin wave propagates into the tropical western Pacific, maintaining the NWPAC through Ekman divergence and suppressed convection (Yang et al. 2007; Wu et al. 2009; Xie et al. 2009; Yang et al. 2010). Xie et al. (2016) revealed that a cross-basin coupled ocean–atmosphere mode combining the above two physical processes has coherent climate effects on East Asia summer climate.

However, some previous studies argued that the preceding El Niño and subsequent TIO warming may not be enough to explain the circulation anomalies over the

NWP, and they suggested that cold SST anomalies in tropical central-eastern Pacific (TCEP) also contribute to NWPAC by triggering a pair of anticyclonic Rossby waves on both sides of the equator (Fan et al. 2013). Moreover, some other studies emphasized the role of the warm SST anomalies around the Maritime Continent (MC), which can drive local Hadley circulation anomaly with descending anomalies over the NWP and strength the NWPAC anomalies (He and Wu 2014; Lu et al. 2006; Sui et al. 2007; Chung et al. 2011). The mechanisms of maintaining the NWPAC during the El Niño decaying summer remain controversial to some degree.

The anomalies during all El Niño events are composited nonselectively in most previous studies. However, El Niño events vary from case to case, with complex temporal and spatial diversities. For example, the El Niño events can be classified into two types based on the periodicity of ENSO cycle, as shown in Fig. 1. One is the fast decaying (FD) El Niño, switching its phase in the following boreal summer (Figs. 1a–c). The other is the slow decaying (SD) El Niño with its phase persisting to the following autumn and winter (Figs. 1d–f). The SST anomalies are distinct during the two types of events, which are associated with fundamental different time scales of ENSO and dynamic processes (Kim and Kim 2002; Bejarano and Jin 2008; Yun et al. 2015). The FD El Niño tends to be a quasi-biennial period (2–3 years) oscillation, whereas the SD El Niño is a low-frequency period (3–5 years) oscillation. However, this feature was often neglected in nonselective composite analyses and regression analyses as shown in Figs. 1g–i.

Different El Niño decaying paces could result in diverse SST anomaly pattern in the TIO and tropical Pacific, with different impacts on the NWP circulation anomalies (Chen et al. 2012; Feng et al. 2014). Chen et al. (2012) indicated that an FD El Niño can lead to stronger NWPAC anomalies in the following summer than an SD El Niño. However, the mechanisms of the NWPAC anomalies in different El Niño decaying summers are still controversial. During FD El Niño summers, the NWPAC anomalies can be forced by the warm SST anomalies around the MC (Wu and Zhou 2008; Chung et al. 2011) or the cold SST anomalies in the TCEP (Wang et al. 2013), or by both of them (Chen and Zhou 2014; Chen et al. 2016). However, Chen et al. (2012) emphasized the cooperative role of warm TIO SST anomalies and cold TCEP SST anomalies in the NWPAC anomalies during FD El Niño summers. During SD El Niño summers, Wu and Zhou (2008) emphasized the role of unabated warm TCEP SST anomalies in sustaining the NWPAC anomalies through enhancing local convection and suppressing convection over the NWP. Chung et al.

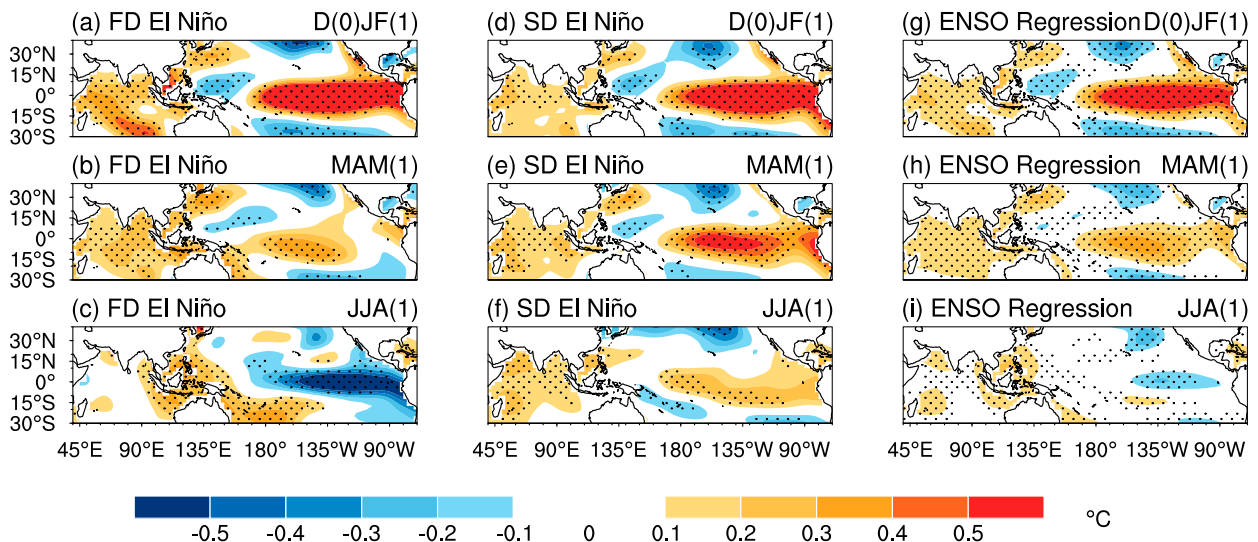


FIG. 1. Composite SST anomalies of FD El Niños from (a) D(0)JF(1) to (c) JJA(1). (d)–(f) As in (a)–(c), but for the SD El Niños composite. (g)–(i) Regressed SST anomalies from D(0)JF(1) to JJA(1) on the D(0)JF(1) standardized Niño-3.4 index. The black dots indicate where the significance exceeds the 90% confidence level.

(2011) and Wang et al. (2013) indicated that the NWPAC anomalies are primarily maintained by the local air–sea interaction, while Chen and Zhou (2014) suggested that warm SST anomalies in the TIO play a crucial role in developing the NWPAC anomalies. Chen et al. (2012) suggested that the positive SST anomalies in the TIO and TCEP have opposite roles in the NWPAC anomalies during SD El Niño cases.

In the present work, we try to figure out which of the above-mentioned mechanisms plays a leading role in maintaining the NWPAC anomalies in the two types of El Niño decaying summers through observational analyses and a suite of numerical experiments by using an atmospheric general circulation model (AGCM). By studying the roles of SST anomalies of various ocean basins in the NWPAC anomalies, we can indirectly demonstrate the roles of the abovementioned air–sea coupled mechanisms in the NWPAC anomalies. The rest of the paper is organized as follows. Section 2 briefly describes the data, methods, and experiment designs. Section 3 outlines the characteristics of SST anomalies, atmospheric circulation anomalies, and possible mechanisms. Section 4 presents the results of numerical experiments and addresses the role of SST anomalies in various oceans. Section 5 delineates the different summer climate effects on China during different El Niño decaying summers. A summary and discussion are given in section 6.

2. Data and methods

The monthly mean atmospheric variables, including wind, geopotential height, and air temperature, are from

the National Centers for Environment Prediction (NCEP)–National Center for Atmospheric Research (NCAR) reanalysis dataset with a horizontal resolution of $2.5^\circ \times 2.5^\circ$, covering the period from 1961 to 2010 (Kalnay et al. 1996) (available at <https://www.esrl.noaa.gov/psd/data/gridded/data.ncep.reanalysis.html>). The SST is from the monthly mean Extended Reconstruction of Historical Sea Surface Temperature version 3 (ERSST3) dataset (Smith et al. 2008), which has a horizontal resolution of $2^\circ \times 2^\circ$ (available at <https://www.esrl.noaa.gov/psd/data/gridded/data.noaa.ersst.html>). A monthly rainfall dataset of 718 stations in China for the period 1961–2010 is provided by the Chinese Meteorological Administration.

We denote the El Niño developing year as year 0 and the following year as year 1. Thus, the El Niño mature winter [December–February (DJF)] is symbolized as D(0)JF(1), the following spring [March–May (MAM)] as MAM(1), and the following summer [June–August (JJA)] as JJA(1). All data are interpolated into the same $2.5^\circ \times 2.5^\circ$ grid. The linear trend, the annual cycle, and a 13-yr running mean are removed to extract interannual variability.

The El Niño cases are selected when the standardized D(0)JF(1) Niño-3.4 SST index (the averaged SST anomaly of 5°S – 5°N and 120° – 170°W) is greater than 0.5. As shown in Fig. 2, the Niño-3.4 SST anomalies in most of cases have evolved to negative in JJA(1), whereas the Niño-4 SST anomalies show large spread in JJA(1). Previous studies suggested that the atmospheric anomalies are more sensitive to Niño-4 SST anomalies than Niño-3.4 SST anomalies due to the higher climatology SST in Niño-4 regions (Zheng et al. 2014). Thus, to better

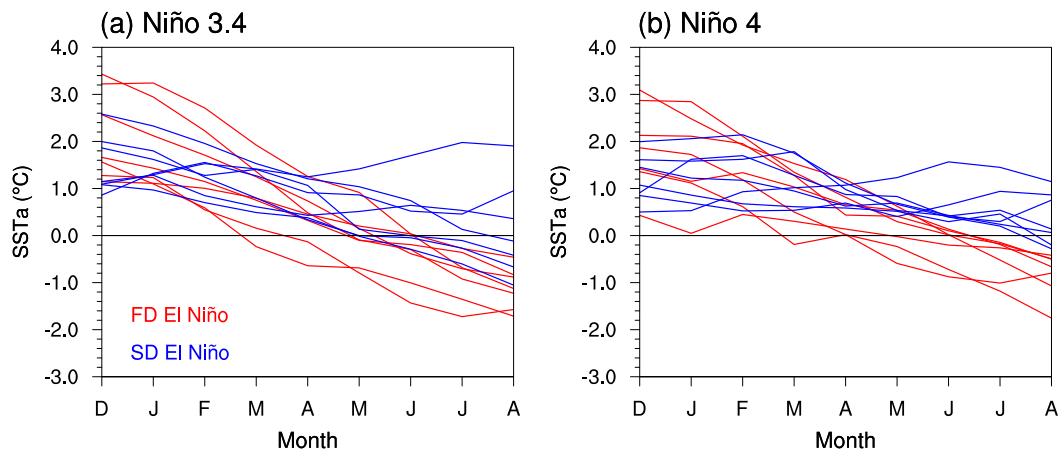


FIG. 2. Composite evolution of the (a) Niño-3.4 index and (b) Niño-4 index for the FD El Niños (red lines) and SD El Niños (blue lines).

reflect the effects of El Niño decay paces on the atmosphere, we select the normalized JJA(1) Niño-4 index to classify the FD and SD El Niño cases, which is similar to the classification in Tao et al. (2017). The cases with negative JJA(1) Niño-4 index (the averaged SST anomaly of 5°S – 5°N and 160°E – 150°W) are classified as FD El Niños, whereas the others as SD El Niños. The classification of all El Niño cases is shown in Table 1. We can find that the JJA(1) Niño-3.4 SSTs in the FD and SD cases are not well separated (Fig. 2a), when the FD and SD cases are classified by Niño-4 index. The significantly separated atmospheric response to the FD and SD cases in the following analyses indicates that the Niño-4 index is a sensitive criterion to present the atmospheric response to El Niño SST anomalies. Because of the limitations of observation data (1961–2010), the number of cases is seven in each type. Therefore, we do not classify El Niño events into more types as in Chowdary et al. (2017). Composite analysis was used in this study, and the statistical significance was estimated with a two-tailed Student's t test.

3. Observational analyses

a. SST anomalies and NWP circulation anomalies

The SST anomaly evolution from the El Niño mature winter to the following summer is shown in Fig. 1. The

regressed El Niño-related SST anomalies in the TCEP gradually decay from the El Niño mature winter to the following spring and summer (Figs. 1g–i). By the subsequent summer, the warm SST anomaly signals in the equatorial eastern Pacific have almost dissipated, and primary SST anomalies are concentrated in the tropical Indo-western Pacific (Fig. 1i). Most previous studies paid attention to the role of the tropical Indo-western Pacific SST anomalies in maintaining the NWPAC anomalies and demonstrated the leading role of the Indo-western Pacific Ocean capacitor in El Niño decaying summers (e.g., Xie et al. 2009; Kosaka et al. 2013). As stated in the introduction, the evolution of El Niño-related SST anomalies shows conspicuous difference during the two types of El Niño decaying years. SST anomalies in the TCEP and the TIO decline fast and switch sign during the FD El Niño following spring and summer, displaying a cold–warm–cold SST anomaly pattern in the TIO, the MC, and the TCEP (Fig. 1c). In comparison, warm SST anomalies in the TCEP and the TIO persist to the decaying summer in SD El Niño cases, displaying a warm–cold–warm SST anomaly pattern in the tropical Indian Ocean and Pacific.

Despite the distinct SST anomaly pattern during two types of El Niño decaying summers, there is still an anomalous anticyclone over the NWP (10° – 35°N ,

TABLE 1. The definitions of FD El Niño and SD El Niño, and corresponding selected years for the period of 1961–2010.

Types	Definitions	Years
FD El Niño	Stn D(0)JF(1) Niño-3.4 > 0.5 Stn JJA(1) Niño-4 < 0	1963/64, 1972/73, 1987/88, 1991/92, 1994/95, 1997/98, 2009/10
SD El Niño	Stn D(0)JF(1) Niño-3.4 > 0.5 Stn JJA(1) Niño-4 > 0	1965/66, 1968/69, 1969/70, 1976/77, 1982/83, 1986/87, 2006/07

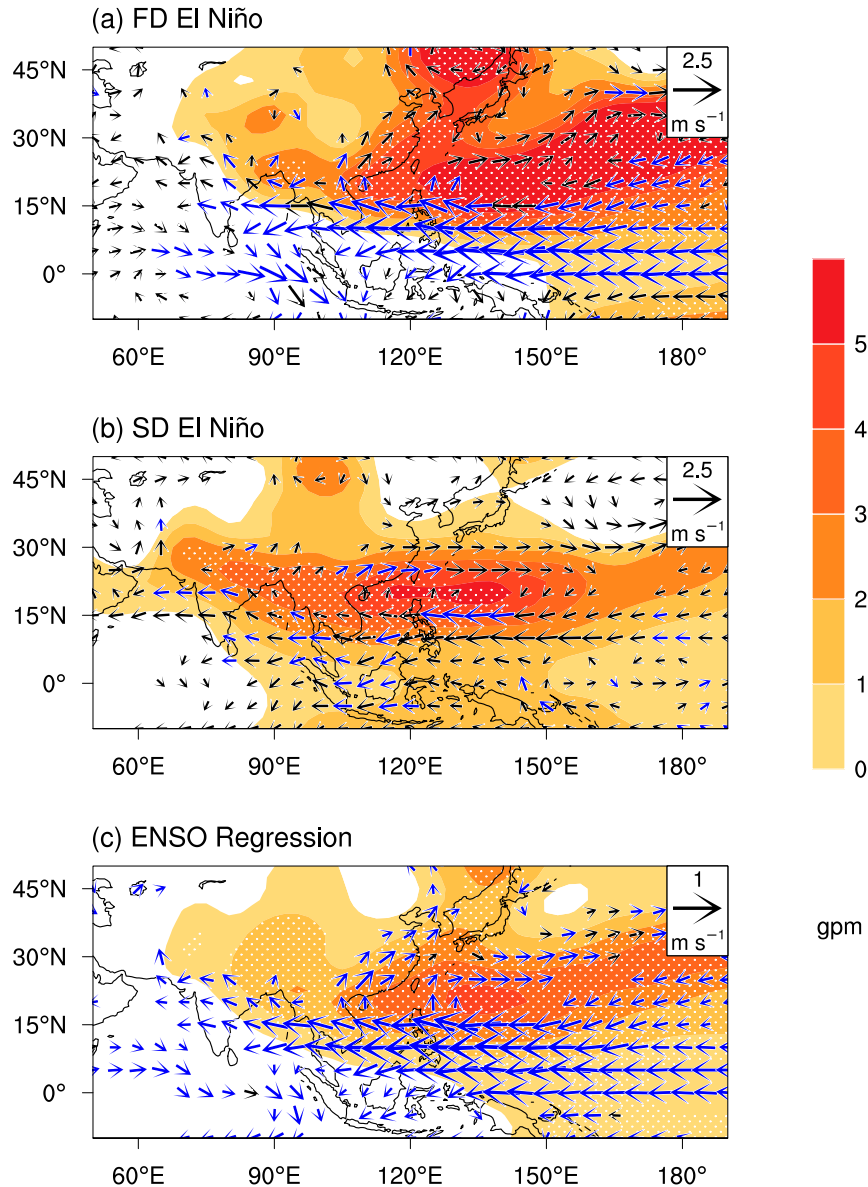


FIG. 3. Composite JJA(1) 850-hPa geopotential height anomalies (shading) and wind anomalies (vectors) in (a) FD ENSO and (b) SD ENSO events. (c) Regressed JJA(1) 850-hPa geopotential height anomalies (shading) and wind anomalies (vectors) on the D(0)JF(1) standardized Niño-3.4 index. The white dots and blue arrows indicate where the significance exceeds the 90% confidence level.

100°E–170°W) during the following summer of both types of El Niño events (Fig. 3). The NWPAC differs conspicuously during two types of El Niño decaying summers. During FD El Niño summers, the southwesterly anomalies to the western flank of the NWPAC anomalies can reach to mid- to high latitudes. The western part of the NWPAC anomalies is located around 10°–25°N, 110°–150°E, and the eastern part extends northeastward. The NWPAC anomalies during SD El Niño summers are weaker and extend

more westward than those during FD El Niño summers. The distinct atmospheric anomalies are embodied in the geopotential height anomalies and the streamfunction anomalies (Fig. 4). The strong NWPAC anomalies during FD El Niño summers and the weaker circulation anomalies during SD El Niño summers are consistent with Chen et al. (2012). The distinct NWPAC anomalies and SST anomalies during two types of El Niño decaying summers imply that the maintenance mechanisms of maintaining NWPAC

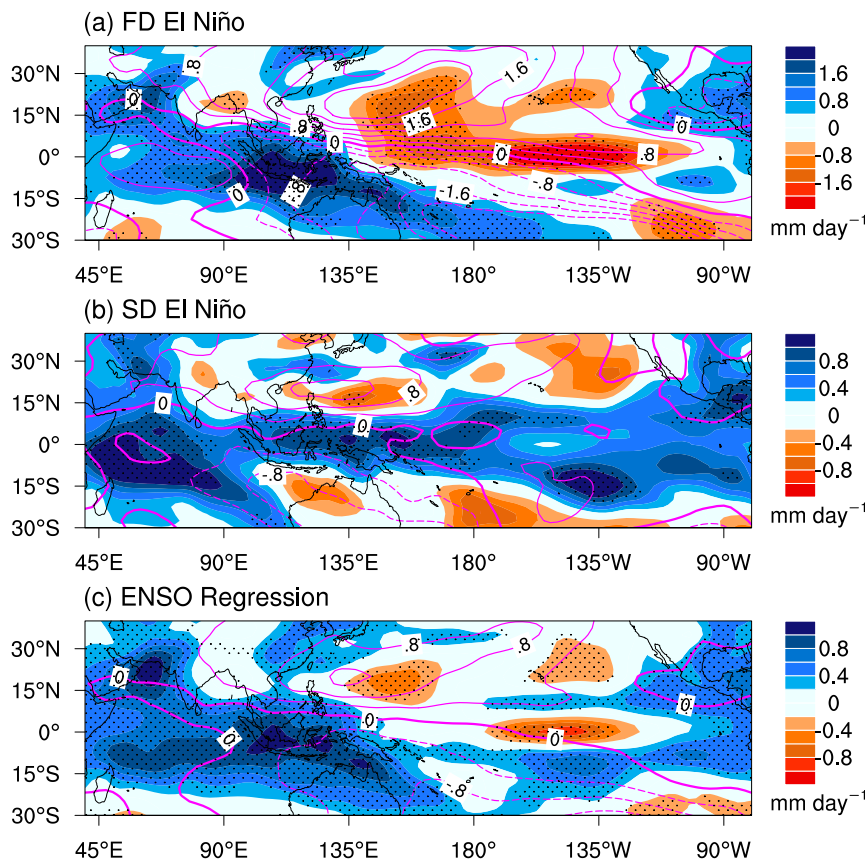


FIG. 4. As in Fig. 3, but for precipitation anomalies (shading) and 850-hPa streamfunction anomalies (contours). The black dots indicate where the significance exceeds the 90% confidence level.

anomalies could be different from each other in the two situations.

b. Systematic tropical circulation anomalies and the formation mechanism of NWPAC anomalies

During FD El Niño summers, enhanced convection and positive rainfall anomalies are centered over the MC corresponding to the warm MC SST anomalies, whereas suppressed convection and negative rainfall anomalies are over the TCEP with cold SST anomalies (Figs. 4a and 1c). In response to heating over the MC region, an eastward propagating Kelvin wave and a pair of westward extended Rossby waves appear on both sides of the equator (Fig. 5a). Correspondingly, anomalous easterlies at 850-hPa flow into the MC (Fig. 3a), and anomalous westerlies at 200 hPa dominate over the MC (Fig. 5a). The warm Kelvin wave propagating into the tropical western Pacific plays an important role in maintaining the NWPAC anomalies through Ekman divergence mechanism (Yang et al. 2007; Wu et al. 2009; Xie et al. 2009; Yang

et al. 2010). Meanwhile, cold SST anomalies in the TCEP trigger an opposite Matsuno–Gill response in tropospheric temperature anomalies. Specifically, a pair of significant cyclone anomalies at high level straddle the equator in the tropical western-central Pacific, and anomalous easterlies at high level are over the tropical eastern Pacific (Fig. 5a). Some studies suggested that the cold SST anomalies in the TCEP also contribute to the development of the NWPAC anomalies through triggering an atmospheric cold Rossby wave (Fan et al. 2013; Wang et al. 2013; Chen et al. 2016). The atmospheric Matsuno–Gill pattern anchored over the MC and the opposite Matsuno–Gill pattern triggered by cold TCEP SST anomalies are coherent over the tropical western Pacific, facilitating the maintaining of the NWPAC.

Previous studies suggested that the heating over the MC can influence the convective anomalies over the NWP through local Hadley circulation changes (He and Wu 2014; Lu et al. 2006; Sui et al. 2007; Wu and Zhou 2008). A 200-hPa anomalous divergence is

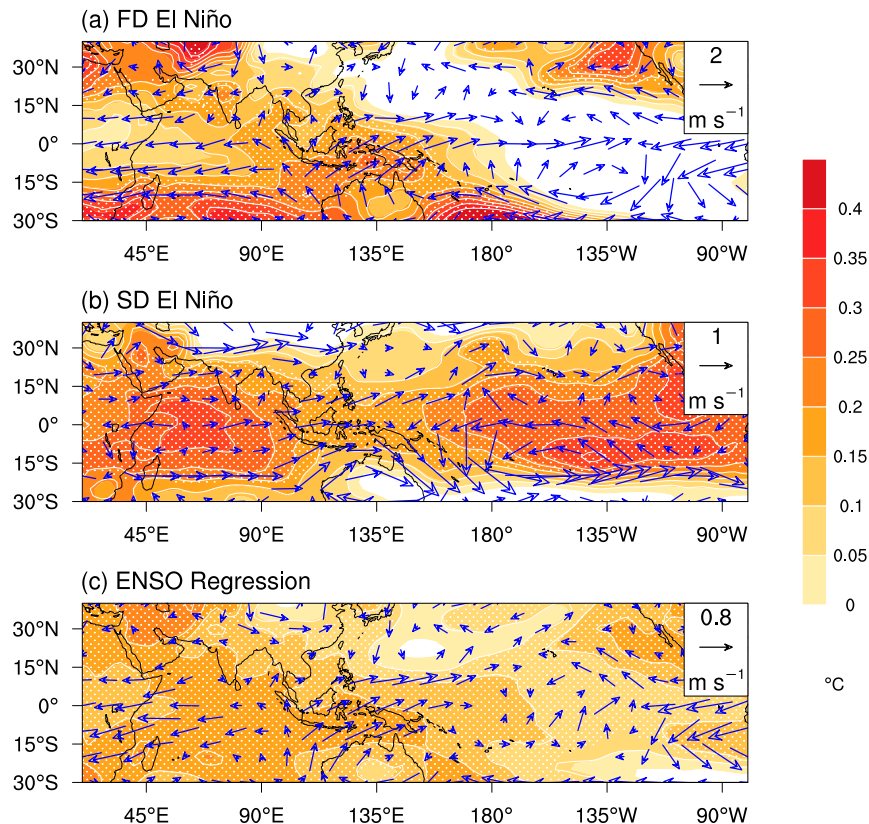


FIG. 5. As in Fig. 3, but for the tropospheric (1000–200 hPa) temperature anomalies (shading) and 200-hPa wind anomalies (vectors). The white dots and blue arrows indicate where the significance exceeds the 90% confidence level.

centered over the MC and the TIO, responding to the convective heating (Figs. 4a and 6a). Figure 7 shows the local Hadley circulation anomalies, which is defined as meridional divergent wind and vertical velocity averaged from 95° to 140°E (Zhao and Moore 2008). Ascending motion over the MC and descending motion over the NWP are significant (Figs. 6a and 7a), indicative of an enhanced Hadley circulation, which is conducive to developing of the NWPAC anomalies.

In conclusion, the warm MC SST anomalies contribute to maintaining of the NWPAC anomalies through the warm Kelvin wave and strengthened Hadley circulation anomalies, and the cold TCEP SST anomalies also facilitate development of NWPAC anomalies by the atmospheric Rossby wave. However, the relative contributions of the MC SST anomalies and the TCEP SST anomalies cannot be determined in the observational analyses, which will be explored by numerical models in the next section.

During SD El Niño summers, the basinwide warming in the TIO generates strong positive precipitation anomalies (Figs. 1f and 4b), which trigger an atmospheric

Matsuno–Gill response over the TIO (Fig. 5b). The TIO Matsuno–Gill pattern during SD El Niño summers is more westward than that over the MC during FD El Niño summers (Fig. 4a), which may explain why the NWPAC anomalies can extend more westward in SD El Niño summers than those in FD El Niño summers. The warm SST anomalies in the TCEP also trigger a warm atmospheric Matsuno–Gill response. A pair of strong anticyclonic anomalies, as a Rossby wave response to convective heating in the TCEP, straddles the equator in the TCEP, and the resultant equatorial easterlies collide with the westerlies over the tropical western Pacific. Based on previous studies, the warm SST anomalies in the TCEP generate an atmospheric warm Rossby wave, which does not facilitate the NWPAC anomalies (Fan et al. 2013; Wang et al. 2013; Chen et al. 2016). Meanwhile, the basin warming in the TIO may play a leading role in maintaining the NWPAC anomalies during the SD El Niño summers (Yang et al. 2007; Wu et al. 2009; Xie et al. 2009; Yang et al. 2010).

During SD El Niño summers, the large-scale divergent circulation pattern differs conspicuously from

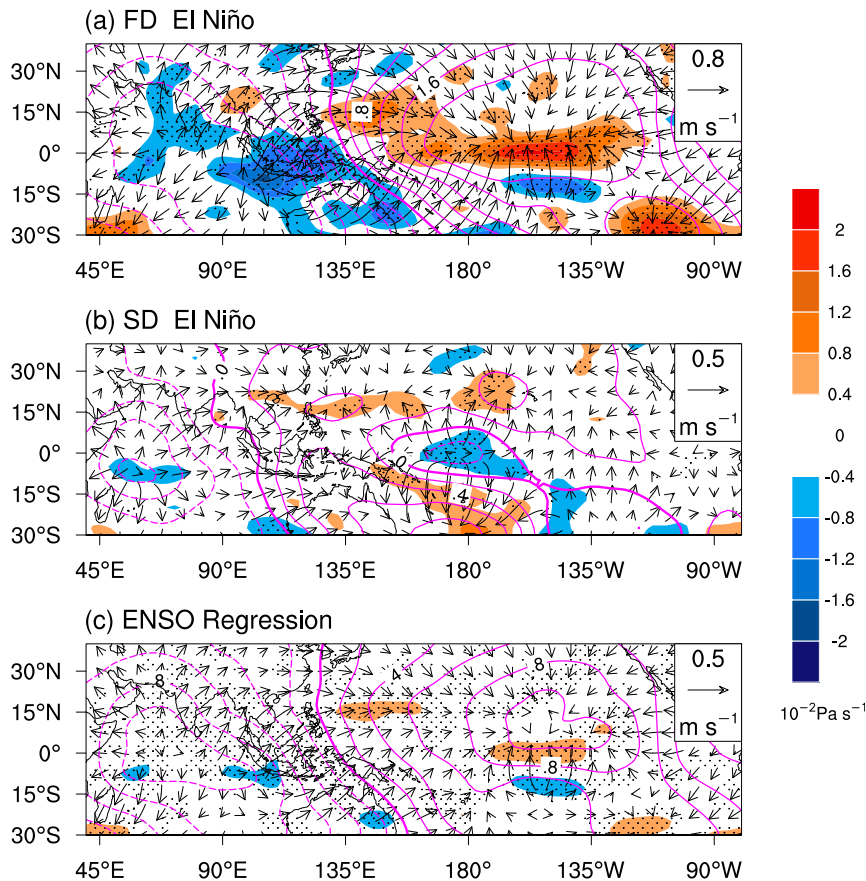


FIG. 6. As in Fig. 3, but for JJA(1) 200-hPa velocity potential ($10^5 \text{ m}^2 \text{ s}^{-1}$; contours), divergent wind (vectors), and 500-hPa vertical velocity (shading) anomalies. The black dots indicate where the significance exceeds the 90% confidence level.

that in FD El Niño summers. As a response to the convection anomalies in the TIO and the TCEP (Fig. 4b), the Walker circulation is weakened with ascending anomalies over the TIO and the TCEP and descending anomalies over the tropical western Pacific (Fig. 6b). From the meridional circulation anomalies shown in Fig. 7b, strong descending anomalies over the NWP cannot be balanced by the meridional circulation. It implies that the enhanced convection over the TIO and TCEP may contribute to the downward motion over the NWP via the weakened Walker circulation, which is consistent with Wu and Zhou (2008). Overall, the TIO basin warming plays a leading role in maintaining the NWPAC anomalies during SD El Niño summers, while the durative TCEP SST anomalies may be not conducive to the formation of the NWPAC. The role of warm TIO SST anomalies is partly offset by the warm TCEP SST anomalies, resulting in weak circulation anomalies over the NWP during SD El Niño summers.

The JJA(1) regressed anomalies based on the whole period are closer to those in FD El Niño than in

SD El Niño, due to the stronger composited anomalies in FD El Niño (Figs. 3, 4, 6, and 7). The regressed tropospheric temperature anomalies display a significant warm atmospheric Kelvin wave over the TIO and the MC (Fig. 5c). However, the atmospheric Matsuno–Gill response over the TCEP is negligible, which may be attributed to the offset of the opposite Matsuno–Gill patterns over the TCEP in FD El Niño summers and in SD El Niño summers. These results illustrate that the roles of TCEP SST anomalies in modulating the NWPAC anomalies in different types of El Niño decaying summers are obscured in regression analyses.

4. Numerical experiments

Because of the complex superposed effects of SST anomalies over various basins, some atmospheric patterns suggested in the last section cannot be identified very clearly in the observational analyses. To further identify the contributions of SST anomalies in various

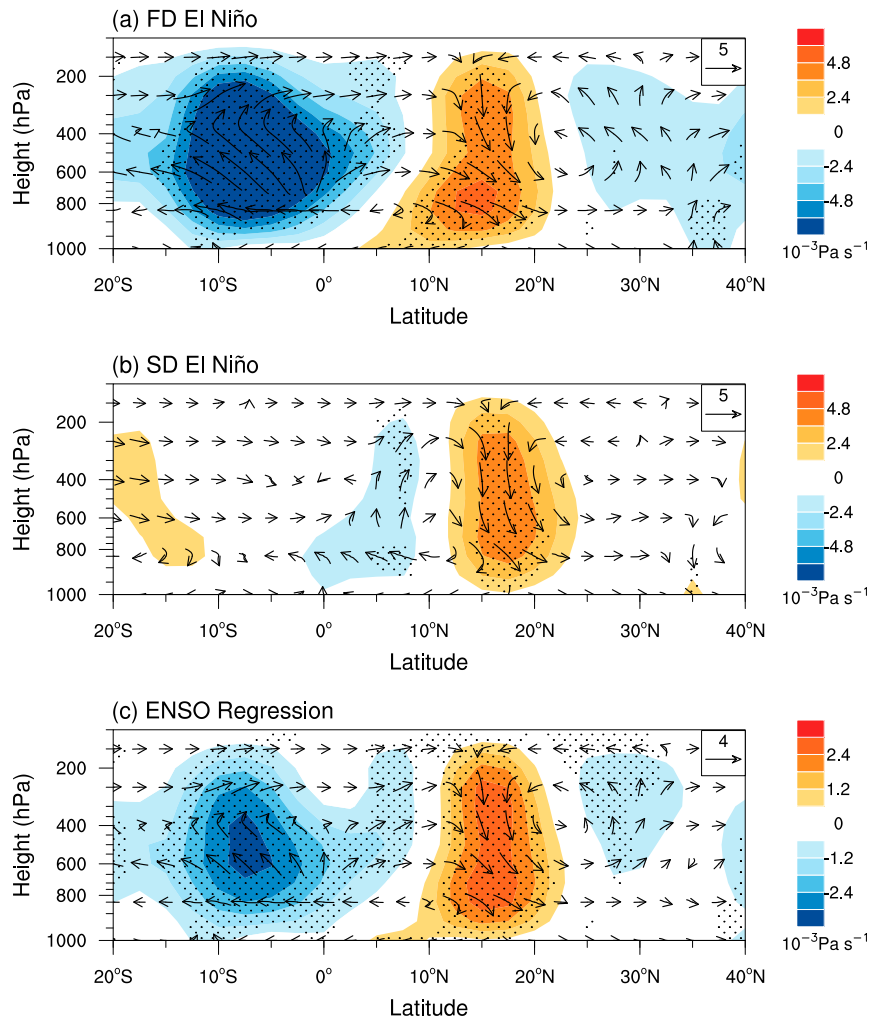


FIG. 7. As in Fig. 3, but for JJA(1) vertical velocity (shading) and meridional velocity averaged over 95°–140°E. The black dots indicate where the significance exceeds the 90% confidence level.

oceans, we perform a suite of sensitivity experiments using ECHAM5, which is an AGCM from the Max Planck Institute for Meteorology (Roeckner et al. 2003). Although AGCMs cannot simulate the air–sea coupled processes, which are necessary to the formation of SST and atmospheric anomalies around the tropics during ENSO, AGCMs are effective tools to study the atmospheric response to SST anomalies and indirectly demonstrate the contributions of various air–sea coupled processes (e.g., Wang et al. 2013; Xie et al. 2016).

One is a control run (referred to simply as Control) in which the SST boundary conditions are composed of climatological SST and sea ice with a seasonal cycle. Two sets of sensitivity experiments are conducted with the composited SST anomalies in FD El Niño shown in Figs. 1a–c (referred to as FD_All run) and those in SD

El Niño shown in Figs. 1d–f (referred to as SD_All run), respectively. In FD_All run and SD_All run, these SST anomalies are added to climatological SST in the entire tropics (15°S–15°N) as the SST boundary conditions, respectively. Since significant SST anomalies appear around the MC and in the TCEP during FD El Niño summers and in the TIO and TCEP during SD El Niño summers (Figs. 1a–f), we designed four other sets of sensitivity experiments with the composited SST anomalies with seasonal cycle in these key oceans individually added to the climatological SST, referred to as the FD_MC run, FD_TCEP run, SD_TIO run, and SD_TCEP run, respectively. The details of SST boundary conditions in the seven experiments are summarized in Table 2. Each set of experiments was integrated 40 years, and the results in the last 30 years were averaged to reduce the influence

TABLE 2. Description of control and sensitivity experiments.

Exp. name	SST boundary condition
Control	Climatological SST with seasonal cycle
FD_All	The SST anomalies in the tropics (15°S–15°N) in the composite FD El Niño years from January to December are added on climatological SST
SD_All	Similar to FD-All run, but with SST anomalies from composite SD El Niño years
FD_TCEP	The SST anomalies in the tropical central-eastern Pacific (15°S–15°N, 170°E–100°W) in the composite FD El Niño years from January to December are added on climatological SST
SD_TCEP	Similar to FD-TCEP run, but with SST anomalies from composite SD El Niño years
FD_MC	The SST anomalies in the tropical Maritime Continent (15°S–15°N, 90°–150°E) in the composite FD El Niño years from January to December are added on climatological SST
SD_TIO	The SST anomalies in the tropical Indian Ocean (15°S–15°N, 40°–120°E) in the composite SD El Niño years from January to December are added on climatological SST

of internal variability. The differences between the sensitivity runs and the control run (hereafter denoted as FD_All–Control, SD_All–Control, FD_MC–Control, FD_TCEP–Control, SD_TIO–Control, and SD_TCEP–

Control) represent the individual role of specific SST anomalies in the atmospheric anomalies.

Figure 8 provides the precipitation pattern in the sensitivity experiments, which reflects the anomalous heating forced by SST anomalies to further influence the atmosphere. In FD_All–Control, the positive and negative rainfall anomalies are conspicuous over the MC and TCEP, respectively (Fig. 8a), showing a response to SST forcing in the two regions. In SD_All–Control, strong positive rainfall appears over the TCEP as a response to warm SST forcing in there. It is noteworthy that in Fig. 8b the simulated negative precipitation anomalies over the MC associated with the negative MC SST anomalies differ from the positive anomalies in the observations. The discrepancies could be a result of oversensitive precipitation response to tropical SST anomalies in AGCMs due to the lack of air–sea coupled processes, although the negative MC SST anomalies are quite weak here. In addition, the lack of air–sea coupling in AGCMs could also induce the subtropical system response closer to the equator relative to the observations, which would further induce some other discrepancies such as rainfall anomalies over China (Figs. 8 and 4).

Even though there are some discrepancies between the AGCM-simulated precipitation anomalies and the observations, the FD_All–Control and SD_All–Control

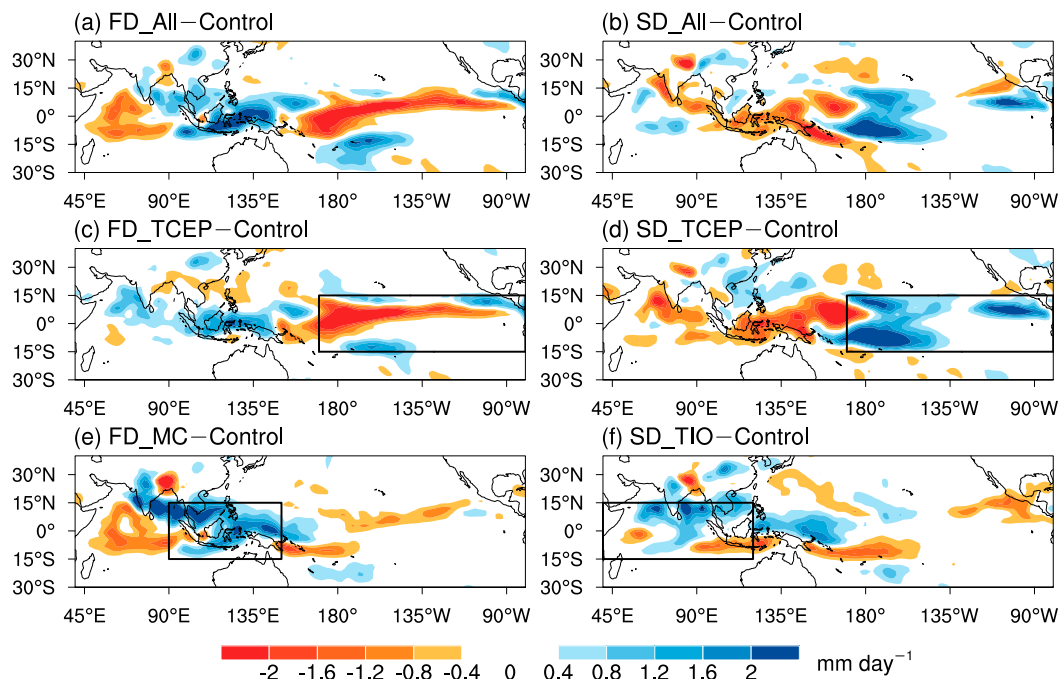


FIG. 8. JJA(1) precipitation (shading) in (a) FD_All–Control, (b) SD_All–Control, (c) FD_TCEP–Control, (d) SD_TCEP–Control, (e) FD_MC–Control, and (f) SD_TIO–Control. The JJA(1) SST forcing is the composited SST anomalies shown in Figs. 1c and 1f in the entire tropics (15°S–15°N) in (a) and (b). The black boxes in (c)–(f) highlight the SST forcing region.

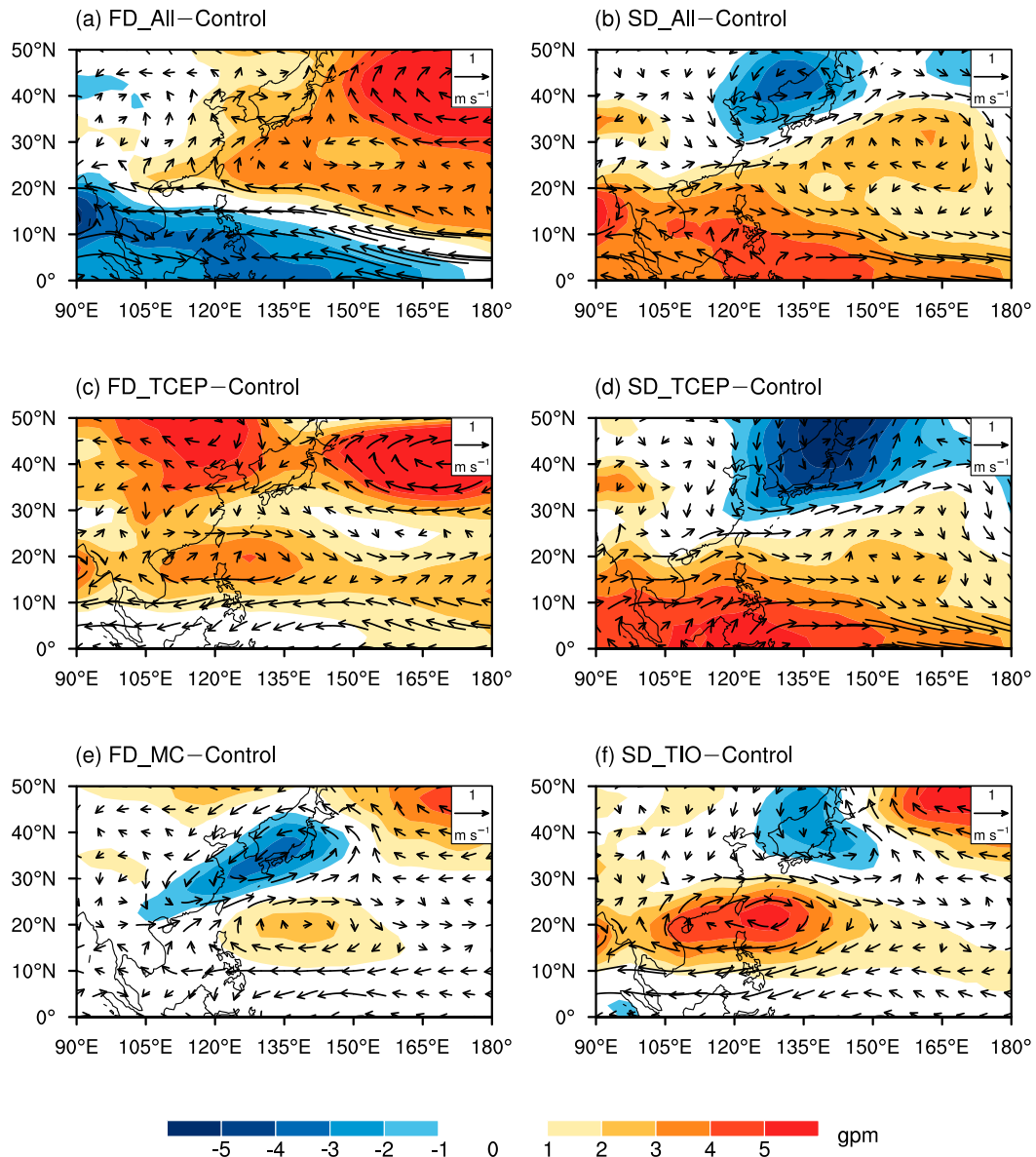


FIG. 9. Difference of 850-hPa winds (vectors) and geopotential height (shading) in JJA(1) between (a) FD_All, (b) SD_All, (c) FD_TCEP, (d) SD_TCEP, (e) FD_MC, and (f) SD_TIO, respectively, and Control run.

quite realistically reproduce the features of observed NWPAC anomalies in FD and SD El Niño summers (Figs. 3a,b and 9a,b), respectively, including the easterly wind anomalies over the tropical Indo-western Pacific, the northward extension of southwesterly anomalies, and the northeastward extension of the NWPAC anomalies during FD El Niño summers and the weaker NWPAC anomalies and the cyclonic anomalies on their northern side during SD El Niño summers. Tropical tropospheric temperature and 200-hPa wind anomalies are also very similar to those in observations (Figs. 5a,b and 10a,b), featuring an atmospheric Matsuno–Gill response to tropical SST anomalies. The realistic responses in

FD_All–Control and SD_All–Control suggest that the circulation anomalies in the NWP are primarily forced by tropical SST anomalies, which is consistent with some previous studies (e.g., Wang et al. 2013; Chen et al. 2016; Chen et al. 2017; Chen et al. 2019). The well-reproduced circulation response during SD El Niño summers implies that the discrepant negative rainfall anomalies over the MC in SD_All–Control do not contribute much to the circulation anomalies.

In FD_TCEP–Control, prominent negative precipitation anomalies emerge over the TCEP due to the cold TCEP SST forcing (Fig. 8c). As a Rossby wave response to the diabatic cooling, there are prominent

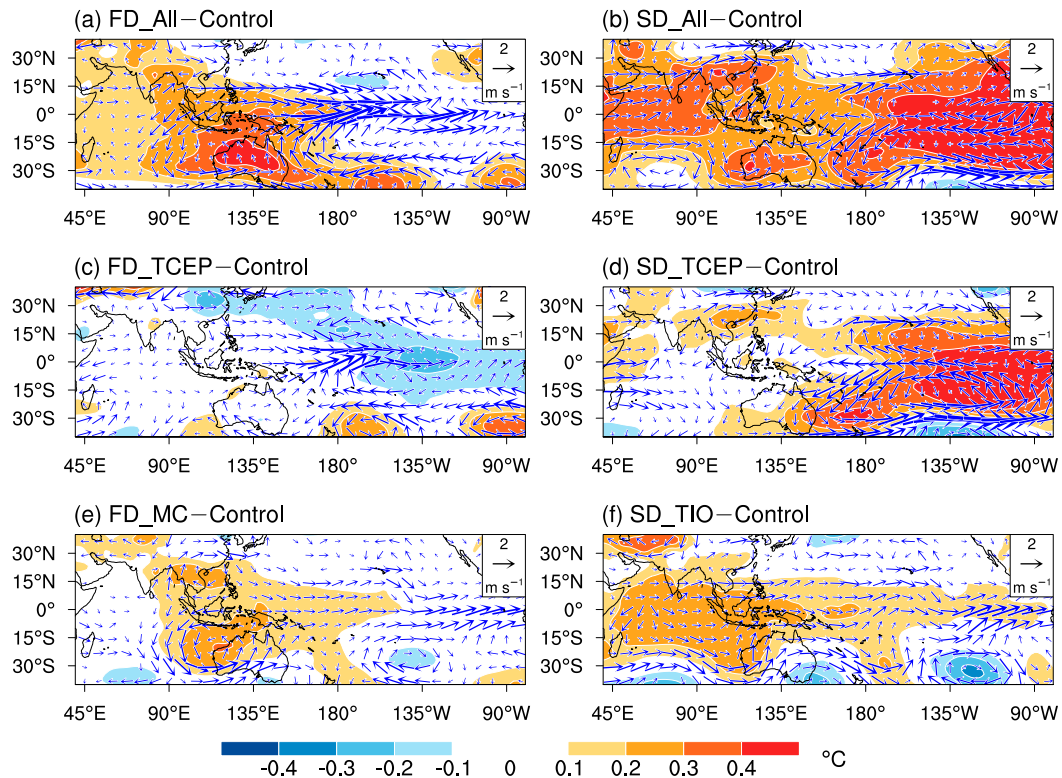


FIG. 10. As in Fig. 9, but for tropospheric (1000–200 hPa) temperature (shading) and 200-hPa winds (vectors).

anticyclonic anomalies and positive geopotential height anomalies over the NWP (Fig. 9c). Meanwhile, an anomalous anticyclone also appears over the NWP in FD_MC-Control (Fig. 9e) as a Kelvin wave response to the diabatic heating in the MC (Fig. 8e). The anomalous upper-level westerlies over the tropical western Pacific as a Kelvin wave response to the heating in the MC are also a response to the cooling in the TCEP (Figs. 10a,c,e). However, the anomalous anticyclone over the NWP in FD_TCEP-Control run is stronger than that in FD_MC-Control run. The results suggest that the NWPAC anomalies are maintained by a combined effect of the MC warming and the TCEP cooling during FD El Niño summers, and the TCEP cooling may play a more important role, which is consistent with Chen et al. (2016).

In SD_TCEP-Control, the warm SST anomalies in the TCEP trigger a pair of anticyclonic anomalies at high levels on both side of the equator (Fig. 10d), and resultant cyclonic wind anomalies and positive rainfall anomalies are generated at low levels (Figs. 8d and 9d). Further, the diabatic heating over the TCEP triggers a Rossby wave train, a positive–negative–positive rainfall pattern extends from the central Pacific to the NWP (Fig. 8d), which is accompanied by cyclonic–anticyclonic–cyclonic wind anomalies from the central Pacific to

the NWP (Fig. 9d). The cyclonic wind anomalies over the western NWP can weaken the western part of the NWPAC anomalies and make the anomalous southwesterlies difficult to extend to high latitudes, while the anticyclonic wind anomalies over the eastern NWP can enhance the eastern part of the NWPAC anomalies. In SD_TIO-Control, warm SST anomalies in the TIO force conspicuous anticyclonic anomalies over the NWP through triggering a warm Kelvin wave (Figs. 9f and 10f; Yang et al. 2007; Wu et al. 2009; Xie et al. 2009; Yang et al. 2010; Chowdary et al. 2011; Chowdary et al. 2016). The anomalous wind and geopotential height over the NWP and the midlatitude are characterized by a Pacific–Japan-like pattern (Nitta 1987; Huang and Lu 1989). Overall, the TIO warming plays a crucial role in maintaining the NWPAC anomalies during SD El Niño summers, and the role of warm TIO SST anomalies is partly offset by the warm SST anomalies in the TCEP, resulting in weak circulation anomalies over the NWP during SD El Niño summers.

5. Impacts on summer rainfall in China

The distinct impacts of different El Niño decaying paces on the NWPAC anomalies could induce different summer rainfall anomalies in China. In all post-ENSO

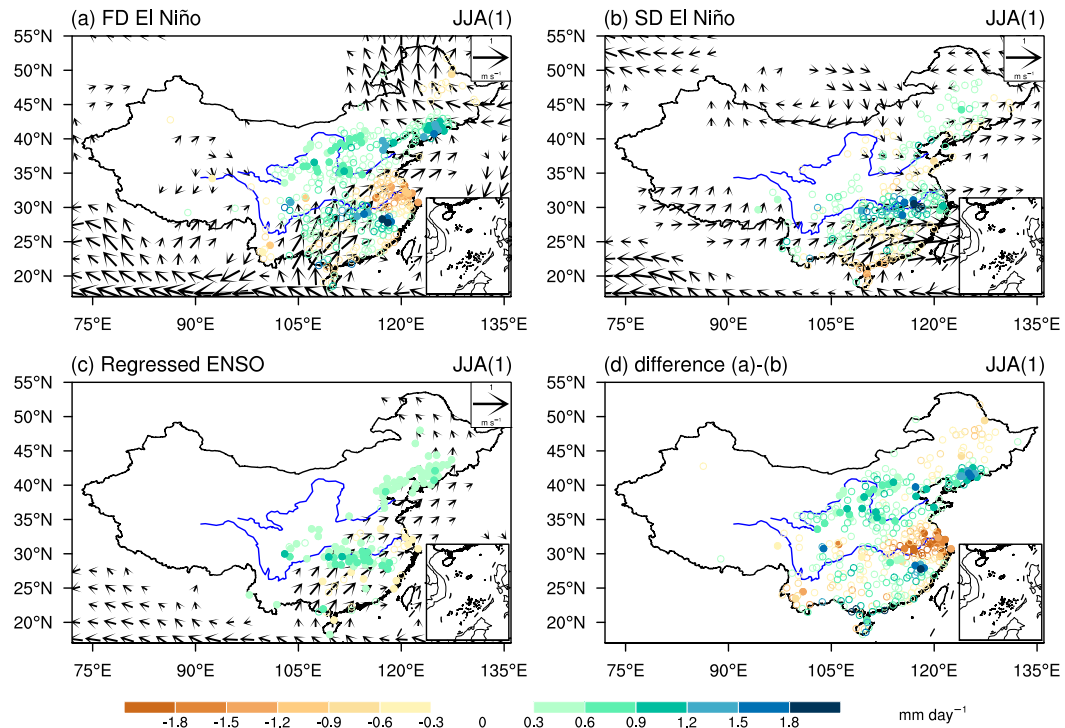


FIG. 11. (a)–(c) As in Fig. 3, but for the rainfall anomalies (dots and circles; the dots indicate stations significant at the 90% confidence level based on the Student's t test) and 850-hPa wind anomalies (vectors). (d) Difference of JJA(1) rainfall anomalies between FD El Niño and SD El Niño.

summers, positive rainfall anomalies are distributed in the Hebei-Liaoning Province, the Yangtze River basin, and the mountainous area of central China (Fig. 11c), consistent with Hu et al. (2017). However, the precipitation anomaly patterns are distinct during different El Niño decaying summers. During FD El Niño summers, significant positive rainfall anomalies are generated over the most areas of northern China and the Yangtze River basin because the strong anomalous southwesterlies of the NWPAC can reach mid- to high latitudes (Fig. 11a). During SD El Niño summers, the weak anomalous southwesterlies of the NWPAC anomalies contribute to transporting water vapor to the Yangtze River basin and the anomalous northerlies on the northern side of the NWPAC anomalies bring cold air, which is conducive to forming positive rainfall anomalies over the Yangtze River basin (Li and Lu 2017). Thus, positive rainfall anomalies are mainly concentrated over the Yangtze River basin during SD El Niño summers (Figs. 3b and 11b). There are larger positive rainfall anomalies in the northern China and negative rainfall anomalies in the downstream of the Yangtze River basin during FD El Niño summers than those during SD El Niño summers (Fig. 11d). Previous studies suggested that the distinct El Niño decaying paces have different impacts on the Indo-Pacific and Korean

peninsula climate (Chowdary et al. 2017; Chen et al. 2018; Yeo et al. 2018). In this study, the distinct summer rainfall anomalies in China also inspire us that more attention should be paid to the El Niño decaying pace in predicting the summer rainfall in China.

6. Summary and discussion

In this study, we investigate the role of the decaying paces of El Niño events in the formation of the NWPAC anomalies during post-El Niño summers. The tropical SST anomalies during El Niño decaying summers are distinct from case to case, which was often omitted in studies of ENSO's impacts. Here, we classified the El Niño events into two groups: the FD El Niños and the SD El Niños. In FD El Niño summers, El Niño has switched to La Niña with apparent cold SST anomalies in the TCEP and warm SST anomalies around the MC, whereas in SD El Niño summers, warm SST anomalies in the TCEP persist to decaying summer and there are basinwide positive SST anomalies in the TIO. Based on the statistical analyses and numerical experiments, we reveal that the El Niño decaying pace is a key factor determining the characteristics, maintaining mechanisms and the effect on China summer rainfall of the NWPAC anomalies.

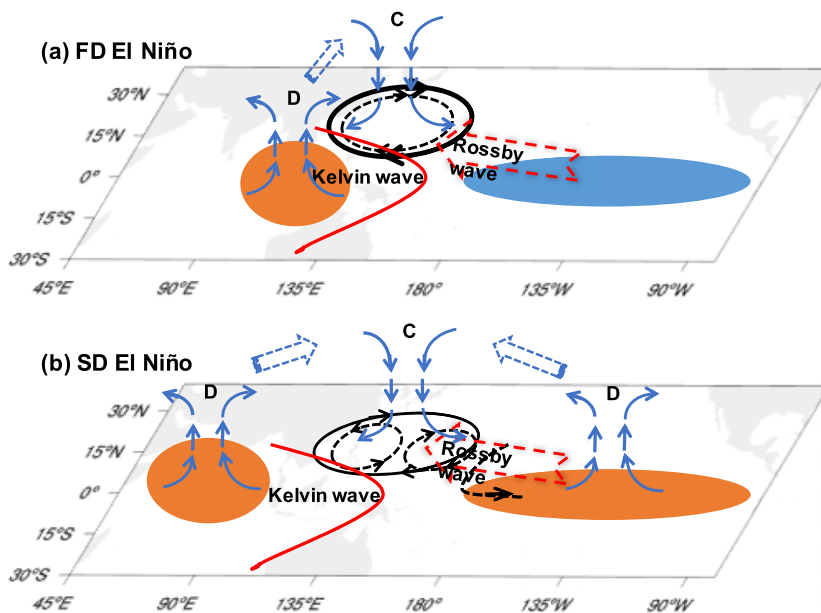


FIG. 12. Schematic diagrams illustrate the mechanisms of JJA(1) NWPAC in (a) FD El Niño events and (b) SD El Niño events. Orange (blue) shading represents warm (cold) SST anomalies induced by Kelvin wave response to warm SST anomalies in the MC in (a) and the TIO in (b). Red solid lines represent anticyclonic anomalies in the MC in (a) and the TIO in (b). Black solid circles denote the NWPAC anomalies and the heavier solid circle in (a) than in (b) presents the stronger NWPAC anomalies in FD El Niño events. Black dashed lines represent circulation anomalies associated with Rossby wave response to SST anomalies in TCEP, and the arrows on the dashed lines represent wind direction. Letters C and D represent convergence and divergence on the upper levels, respectively. The upward and downward blue arrows and dashed blue arrows represent large-scale divergent circulation anomalies.

The mechanisms of maintaining the NWPAC anomalies in two distinct El Niño decaying summers are depicted in the schematics shown in Fig. 12. In the FD El Niño summers (Fig. 12a), the cold SST anomalies in the TCEP play a leading role in maintaining the anomalous NWPAC through triggering a Rossby wave response, and the warm SST anomalies around the MC also facilitate the NWPAC anomalies by forcing a Kelvin wave response and enhancing Hadley circulation anomalies. In the SD El Niño summers (Fig. 12b), the Kelvin wave in response to warm TIO SST anomalies plays a crucial role in maintaining the NWPAC anomalies, whereas the Rossby wave in response to warm TCEP SST anomalies weakens the western part of the NWPAC anomalies and strengthens the eastern part of the NWPAC anomalies. In addition, the descending motion over the NWP, linking to the ascending motion forced by warm TIO SST anomalies and TCEP SST anomalies, could suppress the NWP convection and strengthen the NWPAC anomalies.

The distinct NWPAC anomalies during different El Niño decaying years lead to different summer rainfall anomaly patterns in China. The NWPAC anomalies are weaker during SD El Niño summers than during

FD El Niño summers because of the contribution of cyclonic wind anomalies on the western side of the NWPAC anomalies as the Rossby wave response to the warm TCEP SST anomalies during SD El Niño summers (Fig. 9d). The southwesterly anomalies to the western flank of the NWPAC only extend around 35°N during SD El Niño summers. Correspondingly, anomalous positive rainfall is generated over the Yangzi River basin. The southwesterly anomalies during FD El Niño summers are so strong that they reach mid- to high latitudes and induce more pronounced precipitation anomalies over northern China and the Yangzi River basin.

As reviewed in the introduction, there are various theories emphasizing different aspects of the formation mechanism of the NWPAC anomalies during the post-El Niño summers (Wang et al. 2000; Lu et al. 2006; Sui et al. 2007; Yang et al. 2007; Xie et al. 2009; Yang et al. 2010; Fan et al. 2013; Wang et al. 2013; Stuecker et al. 2015; Li et al. 2017; Wu et al. 2017). These theories seem controversial in some degree. The present study suggests that these distinct theories could just emphasize individual aspects of the formation mechanism of the NWPAC anomalies from the perspective of El Niño's

decaying pace by using a suite of AGCM experiments. For example, the role of the warm SST anomalies in the TIO (Yang et al. 2007; Wu et al. 2009; Xie et al. 2009; Yang et al. 2010) is quite apparent during the SD El Niños but weak during the FD El Niños; the role of the SST anomalies around the MC (Lu et al. 2006; Sui et al. 2007; Chen et al. 2016) is more apparent during the FD than the SD El Niños; and the role of the TCEP SST anomalies (Fan et al. 2013; Wang et al. 2013) were often underestimated due to the offset between different decaying El Niños. Therefore, this study suggests that the decaying pace is a very important factor to understanding the diversity of the decaying impacts of El Niños.

This study emphasized the distinct roles of the different TCEP SST anomalies between the FD and SD El Niño summers in the NWPAC anomalies, showing negative SST anomalies with positive contribution in FD El Niños and positive SST anomalies with negative contribution in SD El Niños. This mechanism is different from the possible positive contribution of the positive TCEP SST anomalies to a similar NWPAC anomalous pattern during boreal spring (Wu et al. 2017). Wu et al. (2017) suggested that the warm SST anomalies over the TCEP deliver dry and low moist enthalpy air into the NWP, suppressing local convection and maintaining the NWPAC anomalies. In contrast, the present study, as in some previous studies (Fan et al. 2013; Wang et al. 2013; Chen et al. 2016), emphasized the role of atmospheric Rossby waves in the east of the NWPAC anomalies, which directly respond to the TCEP SST anomalies during El Niño decaying summer.

The present study only discussed the role of the SST anomalies in various ocean basins by analyzing the reanalysis datasets and performing a suite of AGCM experiments, which provides indirect evidence to the role of various air–sea coupled processes in the NWPAC anomalies. Actually, the atmospheric anomalies could be a part of the result of air–sea coupled processes associated with the SST anomalies, which is not discussed here. How do the distinct tropical SST anomalous patterns form from the El Niño peaking winters to the post–El Niño summers during different paces of El Niño decay? Some previous studies have proposed various mechanisms to explain the formation of SST anomalies outside the TCEP, often based on the linear regression results (Figs. 1g–i). For example, the cold SST anomalies in the NWP are related to the ENSO-induced local wind–evaporation–SST (WES) feedback (Wang et al. 2000); and the TIO basinwide warming is the result of the combined effects of ENSO-induced surface heat flux anomalies (Klein et al. 1999; Lau and Nath 2003; Wu et al. 2008), the

tropical tropospheric temperature mechanism (Chiang and Sobel 2002; Chiang and Lintner 2005), the ocean dynamical processes (Huang and Kinter 2002; Xie et al. 2002), and the antisymmetric pattern of atmospheric circulation (Wu et al. 2008; Du et al. 2009). The patterns of the tropical SST anomalies during different types of El Niño decaying years are inconsistent with the SST anomaly pattern from a linear perspective. It could be a very interesting issue worthy to be studied in the future: how the distinct SST anomaly patterns come from during different El Niño decaying pace and how these existing theories about the SST anomaly formation work from the perspective of El Niño decaying pace.

Acknowledgments. This work was supported by the National Natural Science Foundation of China (41722504 and 41831175), the Fundamental Research Funds for the Central Universities (2018B08314), the National Natural Science Foundation of China (41425019, 41661144016, 41675078, U1502233), the Public Science and Technology Research Funds Projects of Ocean (201505013), and the Youth Innovation Promotion Association of CAS (2016074 and 2018102).

REFERENCES

- Bejarano, L., and F.-F. Jin, 2008: Coexistence of equatorial coupled modes of ENSO. *J. Climate*, **21**, 3051–3067, <https://doi.org/10.1175/2007JCLI1679.1>.
- Chang, C. P., Y. S. Zhang, and T. Li, 2000: Interannual and interdecadal variations of the East Asian summer monsoon and tropical Pacific SSTs. Part I: Roles of the subtropical ridge. *J. Climate*, **13**, 4310–4325, [https://doi.org/10.1175/1520-0442\(2000\)013<4310:IAIVOT>2.0.CO;2](https://doi.org/10.1175/1520-0442(2000)013<4310:IAIVOT>2.0.CO;2).
- Chen, M. Y., J.-Y. Yu, X. Wang, and W. Jiang, 2019: The changing impact mechanisms of a diverse El Niño on the western Pacific subtropical high. *Geophys. Res. Lett.*, **46**, 953–962, <https://doi.org/10.1029/2018GL081131>.
- Chen, W., J.-K. Park, B. Dong, R. Lu, and W.-S. Jung, 2012: The relationship between El Niño and the western north Pacific summer climate in a coupled GCM: Role of the transition of El Niño decaying phases. *J. Geophys. Res.*, **117**, D12111, <https://doi.org/10.1029/2011JD017385>.
- Chen, X. L., and T. J. Zhou, 2014: Relative role of tropical SST forcing in the 1990s periodicity change of the Pacific–Japan pattern interannual variability. *J. Geophys. Res. Atmos.*, **119**, 13 043–13 066, <https://doi.org/10.1002/2014JD022064>.
- Chen, Z., Z. Wen, R. Wu, X. Lin, and J. Wang, 2016: Relative importance of tropical SST anomalies in maintaining the western North Pacific anomalous anticyclone during El Niño to La Niña transition years. *Climate Dyn.*, **46**, 1027–1041, <https://doi.org/10.1007/s00382-015-2630-1>.
- , —, —, and Y. Du, 2017: Roles of tropical SST anomalies in modulating the western north Pacific anomalous cyclone during strong La Niña decaying years. *Climate Dyn.*, **49**, 633–647, <https://doi.org/10.1007/s00382-016-3364-4>.

- , Y. Du, Z. Wen, R. Wu, and C. Wang, 2018: Indo-Pacific climate during the decaying phase of the 2015/16 El Niño: Role of southeast tropical Indian Ocean warming, *50*, 4707–4719, <https://doi.org/10.1007/s00382-017-3899-z>.
- Chiang, J. C. H., and A. H. Sobel, 2002: Tropical tropospheric temperature variations caused by ENSO and their influence on the remote tropical climate. *J. Climate*, **15**, 2616–2631, [https://doi.org/10.1175/1520-0442\(2002\)015<2616:TTVCB>2.0.CO;2](https://doi.org/10.1175/1520-0442(2002)015<2616:TTVCB>2.0.CO;2).
- , and B. R. Lintner, 2005: Mechanisms of remote tropical surface warming during El Niño. *J. Climate*, **18**, 4130–4149, <https://doi.org/10.1175/JCLI3529.1>.
- Chou, C., L. F. Huang, J. Y. Tu, L. S. Tseng, and Y. C. Hsueh, 2009: El Niño impacts on precipitation in the western North Pacific–East Asian sector. *J. Climate*, **22**, 2039–2057, <https://doi.org/10.1175/2008JCLI2649.1>.
- Chowdary, J. S., S.-P. Xie, J.-J. Luo, J. Hafner, S. Behera, Y. Masumoto, and T. Yamagata, 2011: Predictability of northwest Pacific climate during summer and the role of the tropical Indian Ocean. *Climate Dyn.*, **36**, 607–621, <https://doi.org/10.1007/s00382-009-0686-5>.
- , A. Parekh, R. Kakatkar, C. Gnanaseelan, G. Srinivas, P. Singh, and M. K. Roxy, 2016: Tropical Indian Ocean response to the decay phase of El Niño in a coupled model and associated changes in south and East-Asian summer monsoon circulation and rainfall. *Climate Dyn.*, **47**, 831–844, <https://doi.org/10.1007/s00382-015-2874-9>.
- , H. S. Harsha, C. Gnanaseelan, G. Srinivas, A. Parekh, P. Pillai, and C. V. Naidu, 2017: Indian summer monsoon rainfall variability in response to differences in the decay phase of El Niño. *Climate Dyn.*, **48**, 2707–2727, <https://doi.org/10.1007/s00382-016-3233-1>.
- Chung, P.-H., C.-H. Sui, and T. Li, 2011: Interannual relationships between the tropical sea surface temperature and summertime subtropical anticyclone over the western North Pacific. *J. Geophys. Res.*, **116**, D13111, <https://doi.org/10.1029/2010JD015554>.
- Du, Y., S.-P. Xie, G. Huang, and K. Hu, 2009: Role of air–sea interaction in the long persistence of El Niño–induced north Indian Ocean warming. *J. Climate*, **22**, 2023–2038, <https://doi.org/10.1175/2008JCLI2590.1>.
- Fan, L., S. I. Shin, Q. Y. Liu, and Z. Y. Liu, 2013: Relative importance of tropical SST anomalies in forcing East Asian summer monsoon circulation. *Geophys. Res. Lett.*, **40**, 2471–2477, <https://doi.org/10.1002/grl.50494>.
- Feng, J., L. Wang, and W. Chen, 2014: How does the East Asian summer monsoon behave in the decaying phase of El Niño during different PDO phases? *J. Climate*, **27**, 2682–2698, <https://doi.org/10.1175/JCLI-D-13-00015.1>.
- Fu, C., and D. Ye, 1988: The tropical very low-frequency oscillation on interannual scale. *Adv. Atmos. Sci.*, **5**, 369–388, <https://doi.org/10.1007/BF02656760>.
- He, Z., and R. Wu, 2014: Indo-Pacific remote forcing in summer rainfall variability over the South China Sea. *Climate Dyn.*, **42**, 2323–2337, <https://doi.org/10.1007/s00382-014-2123-7>.
- Horel, J. D. and J. M. Wallace, 1981: Planetary-scale atmospheric phenomena associated with the Southern Oscillation. *Mon. Wea. Rev.*, **109**, 813–829, [https://doi.org/10.1175/1520-0493\(1981\)109<0813:PSAPAW>2.0.CO;2](https://doi.org/10.1175/1520-0493(1981)109<0813:PSAPAW>2.0.CO;2).
- , and —, 1982: Reply. *Mon. Wea. Rev.*, **110**, 1497, [https://doi.org/10.1175/1520-0493\(1982\)110<1497:R>2.0.CO;2](https://doi.org/10.1175/1520-0493(1982)110<1497:R>2.0.CO;2).
- Hu, K., S.-P. Xie, and G. Huang, 2017: Orographically anchored El Niño effect on summer rainfall in central China. *J. Climate*, **30**, 10 037–10 045, <https://doi.org/10.1175/JCLI-D-17-0312.1>.
- Huang, B. H., and J. L. Kinter, 2002: Interannual variability in the tropical Indian Ocean. *J. Geophys. Res.*, **107**, 3199, <https://doi.org/10.1029/2001JC001278>.
- Huang, R., and L. Lu, 1989: Numerical simulation of the relationship between the anomaly of subtropical high over East Asia and the convective activities in the western tropical Pacific. *Adv. Atmos. Sci.*, **6**, 202–214, <https://doi.org/10.1007/BF02658016>.
- , and Y. Wu, 1989: The influence of ENSO on the summer climate change in China and its mechanism. *Adv. Atmos. Sci.*, **6**, 21–32, <https://doi.org/10.1007/BF02656915>.
- Kalnay, E., and Coauthors, 1996: The NCEP/NCAR 40-Year Reanalysis Project. *Bull. Amer. Meteor. Soc.*, **77**, 437–471, [https://doi.org/10.1175/1520-0477\(1996\)077<0437:TNYRP>2.0.CO;2](https://doi.org/10.1175/1520-0477(1996)077<0437:TNYRP>2.0.CO;2).
- Kim, K. Y., and Y. Y. Kim, 2002: Mechanism of Kelvin and Rossby waves during ENSO events. *Meteor. Atmos. Phys.*, **81**, 169–189, <https://doi.org/10.1007/s00703-002-0547-9>.
- Klein, S. A., B. J. Soden, and N.-C. Lau, 1999: Remote sea surface temperature variations during ENSO: Evidence for a tropical atmospheric bridge. *J. Climate*, **12**, 917–932, [https://doi.org/10.1175/1520-0442\(1999\)012<0917:RSSTDV>2.0.CO;2](https://doi.org/10.1175/1520-0442(1999)012<0917:RSSTDV>2.0.CO;2).
- Kosaka, Y., S.-P. Xie, N.-C. Lau, and G. A. Vecchi, 2013: Origin of seasonal predictability for summer climate over the northwestern Pacific. *Proc. Natl. Acad. Sci. USA*, **110**, 7574–7579, <https://doi.org/10.1073/pnas.1215582110>.
- Lau, N.-C., and M. J. Nath, 1996: The role of the “atmospheric bridge” in linking tropical Pacific ENSO events to extratropical SST anomalies. *J. Climate*, **9**, 2036–2057, [https://doi.org/10.1175/1520-0442\(1996\)009<2036:TROTBI>2.0.CO;2](https://doi.org/10.1175/1520-0442(1996)009<2036:TROTBI>2.0.CO;2).
- , and —, 2003: Atmosphere–ocean variations in the Indo-Pacific sector during ENSO episodes. *J. Climate*, **16**, 3–20, [https://doi.org/10.1175/1520-0442\(2003\)016<0003:AOVITI>2.0.CO;2](https://doi.org/10.1175/1520-0442(2003)016<0003:AOVITI>2.0.CO;2).
- , and —, 2006: ENSO modulation of the interannual and intraseasonal variability of the East Asian monsoon—A model study. *J. Climate*, **19**, 4508–4530, <https://doi.org/10.1175/JCLI3878.1>.
- Li, T., B. Wang, B. Wu, T. J. Zhou, C. P. Chang, and R. H. Zhang, 2017: Theories on formation of an anomalous anticyclone in western North Pacific during El Niño: A review. *J. Meteor. Res.*, **31**, 987–1006, <https://doi.org/10.1007/s13351-017-7147-6>.
- Li, X., and R. Lu, 2017: Extratropical factors affecting the variability in summer precipitation over the Yangtze River basin. *J. Climate*, **30**, 8357–8374, <https://doi.org/10.1175/JCLI-D-16-0282.1>.
- Lin, Z. D., and R. Y. Lu, 2009: The ENSO’s effect on eastern China rainfall in the following early summer. *Adv. Atmos. Sci.*, **26**, 333–342, <https://doi.org/10.1007/s00376-009-0333-4>.
- Lu, R., Y. Li, and B. Dong, 2006: External and internal summer atmospheric variability in the western North Pacific and East Asia. *J. Meteor. Soc. Japan*, **84**, 447–462, <https://doi.org/10.2151/jmsj.84.447>.
- Nitta, T., 1987: Convective activities in the tropical western Pacific and their impact on the Northern Hemisphere summer circulation. *J. Meteor. Soc. Japan*, **65**, 373–390, https://doi.org/10.2151/jmsj1965.65.3_373.
- Roeckner, E., and Coauthors, 2003: The atmospheric general circulation model ECHAM 5. Part I: Model description. MPI Tech. Rep. 349, 127 pp.
- Ropelewski, C. F., and M. S. Halpert, 1987: Global and regional scale precipitation patterns associated with the El Niño/Southern

- Oscillation. *Mon. Wea. Rev.*, **115**, 1606–1626, [https://doi.org/10.1175/1520-0493\(1987\)115<1606:GARSPP>2.0.CO;2](https://doi.org/10.1175/1520-0493(1987)115<1606:GARSPP>2.0.CO;2).
- Smith, T. M., R. W. Reynolds, T. C. Peterson, and J. Lawrimore, 2008: Improvements to NOAA's historical merged land-ocean surface temperature analysis (1880–2006). *J. Climate*, **21**, 2283–2296, <https://doi.org/10.1175/2007JCLI2100.1>.
- Stuecker, M. F., F.-F. Jin, A. Timmermann, and S. McGregor, 2015: Combination mode dynamics of the anomalous northwest Pacific anticyclone. *J. Climate*, **28**, 1093–1111, <https://doi.org/10.1175/JCLI-D-14-00225.1>.
- Sui, C.-H., P.-H. Chung, and T. Li, 2007: Interannual and interdecadal variability of the summertime western North Pacific subtropical high. *Geophys. Res. Lett.*, **34**, L11701, <https://doi.org/10.1029/2006GL029204>.
- Tao, W., G. Huang, R. Wu, K. Hu, P. Wang, and D. Chen, 2017: Asymmetry in summertime atmospheric circulation anomalies over the northwest Pacific during decaying phase of El Niño and La Niña. *Climate Dyn.*, **49**, 2007–2023, <https://doi.org/10.1007/s00382-016-3432-9>.
- Wang, B., R. G. Wu, and X. H. Fu, 2000: Pacific–East Asian teleconnection: How does ENSO affect East Asian climate? *J. Climate*, **13**, 1517–1536, [https://doi.org/10.1175/1520-0442\(2000\)013<1517:PEATHD>2.0.CO;2](https://doi.org/10.1175/1520-0442(2000)013<1517:PEATHD>2.0.CO;2).
- , —, and T. Li, 2003: Atmosphere–warm ocean interaction and its impacts on Asian–Australian monsoon variation. *J. Climate*, **16**, 1195–1211, [https://doi.org/10.1175/1520-0442\(2003\)16<1195:AOIAII>2.0.CO;2](https://doi.org/10.1175/1520-0442(2003)16<1195:AOIAII>2.0.CO;2).
- , B. Q. Xiang, and J.-Y. Lee, 2013: Subtropical high predictability establishes a promising way for monsoon and tropical storm predictions. *Proc. Natl. Acad. Sci. USA*, **110**, 2718–2722, <https://doi.org/10.1073/pnas.1214626110>.
- Webster, P. J., V. O. Magana, T. N. Palmer, J. Shukla, R. A. Tomas, M. Yanai, and T. Yasunari, 1998: Monsoons: Processes, predictability, and the prospects for prediction. *J. Geophys. Res. Oceans*, **103**, 14 451–14 510, <https://doi.org/10.1029/97JC02719>.
- Wu, B., and T. Zhou, 2008: Oceanic origin of the interannual and interdecadal variability of the summertime western Pacific subtropical high. *Geophys. Res. Lett.*, **35**, L13701, <https://doi.org/10.1029/2008GL034584>.
- , —, and T. Li, 2009: Seasonally evolving dominant interannual variability modes of East Asian climate. *J. Climate*, **22**, 2992–3005, <https://doi.org/10.1175/2008JCLI2710.1>.
- , T. Li, and T. Zhou, 2010: Relative contributions of the Indian Ocean and local SST anomalies to the maintenance of the western North Pacific anomalous anticyclone during the El Niño decaying summer. *J. Climate*, **23**, 2974–2986, <https://doi.org/10.1175/2010JCLI3300.1>.
- , T. Zhou, and T. Li, 2017: Atmospheric dynamic and thermodynamic processes driving the western north Pacific anomalous anticyclone during El Niño. Part I: Maintenance mechanisms. *J. Climate*, **30**, 9621–9635, <https://doi.org/10.1175/JCLI-D-16-0489.1>.
- Wu, R., Z.-Z. Hu, and B. P. Kirtman, 2003: Evolution of ENSO-related rainfall anomalies in East Asia. *J. Climate*, **16**, 3742–3758, [https://doi.org/10.1175/1520-0442\(2003\)016<3742:EOERAI>2.0.CO;2](https://doi.org/10.1175/1520-0442(2003)016<3742:EOERAI>2.0.CO;2).
- , B. P. Kirtman, and V. Krishnamurthy, 2008: An asymmetric mode of tropical Indian Ocean rainfall variability in boreal spring. *J. Geophys. Res.*, **113**, D05104, <https://doi.org/10.1029/2007JD009316>.
- Xie, S.-P., H. Annamalai, F. A. Schott, and J. P. McCreary, 2002: Structure and mechanisms of south Indian Ocean climate variability. *J. Climate*, **15**, 864–878, [https://doi.org/10.1175/1520-0442\(2002\)015<0864:SAMOSI>2.0.CO;2](https://doi.org/10.1175/1520-0442(2002)015<0864:SAMOSI>2.0.CO;2).
- , K. Hu, J. Hafner, H. Tokinaga, Y. Du, G. Huang, and T. Sampe, 2009: Indian Ocean capacitor effect on Indo-western Pacific climate during the summer following El Niño. *J. Climate*, **22**, 730–747, <https://doi.org/10.1175/2008JCLI2544.1>.
- , Y. Kosaka, Y. Du, K. M. Hu, J. Chowdary, and G. Huang, 2016: Indo-western Pacific Ocean capacitor and coherent climate anomalies in post-ENSO summer: A review. *Adv. Atmos. Sci.*, **33**, 411–432, <https://doi.org/10.1007/s00376-015-5192-6>.
- Yang, J., Q. Liu, S.-P. Xie, Z. Liu, and L. Wu, 2007: Impact of the Indian Ocean SST basin mode on the Asian summer monsoon. *Geophys. Res. Lett.*, **34**, L02708, <https://doi.org/10.1029/2006GL028571>.
- , —, and Z. Liu, 2010: Linking observations of the Asian monsoon to the Indian Ocean SST: Possible roles of Indian Ocean basin mode and dipole mode. *J. Climate*, **23**, 5889–5902, <https://doi.org/10.1175/2010JCLI2962.1>.
- Yeo, S.-R., S.-W. Yeh, Y. Kim, and S.-Y. Yim, 2018: Monthly climate variation over Korea in relation to the two types of ENSO evolution. *Int. J. Climatol.*, **38**, 811–824, <https://doi.org/10.1002/joc.5212>.
- Yun, K.-S., K.-J. Ha, S.-W. Yeh, B. Wang, and B. Xiang, 2015: Critical role of boreal summer North Pacific subtropical highs in ENSO transition. *Climate Dyn.*, **44**, 1979–1992, <https://doi.org/10.1007/s00382-014-2193-6>.
- Zhang, R. H., A. Sumi, and M. Kimoto, 1996: Impact of El Niño on the East Asian monsoon: A diagnostic study of the '86/87 and '91/92 events. *J. Meteor. Soc. Japan*, **74**, 49–62, https://doi.org/10.2151/jmsj1965.74.1_49.
- , A. Sumi, and M. Kimoto, 1999: A diagnostic study of the impact of El Niño on the precipitation in China. *Adv. Atmos. Sci.*, **16**, 229–241, <https://doi.org/10.1007/BF02973084>.
- Zhang, W., and Coauthors, 2016: Unraveling El Niño's impact on the East Asian monsoon and Yangtze River summer flooding. *Geophys. Res. Lett.*, **43**, 11 375–11 382, <https://doi.org/10.1002/2016GL071190>.
- Zhao, H., and G. W. K. Moore, 2008: Trends in the boreal summer regional Hadley and Walker circulations as expressed in precipitation records from Asia and Africa during the latter half of the 20th century. *Int. J. Climatol.*, **28**, 563–578, <https://doi.org/10.1002/joc.1580>.
- Zheng, F., X.-H. Fang, J.-Y. Yu, and J. Zhu, 2014: Asymmetry of the Bjerknes positive feedback between the two types of El Niño. *Geophys. Res. Lett.*, **41**, 7651–7657, <https://doi.org/10.1002/2014GL062125>.